


Purely spatial diffusion of H atoms in solid normal- and para-hydrogen filmsS. Sheludiakov *Department of Physics and Astronomy, University of Pittsburgh, Pittsburgh, Pennsylvania 15260, USA*D. M. Lee and V. V. Khmelenko *Institute for Quantum Science and Engineering, Department of Physics and Astronomy, Texas A&M University, College Station, Texas 77843, USA*

Yu. A. Dmitriev

Ioffe Institute, 26 Politekhnikeskaya, St. Petersburg 194021, Russian Federation

J. Järvinen, J. Ahokas, and S. Vasiliev

Department of Physics and Astronomy, University of Turku, 20014 Turku, Finland

(Received 2 March 2022; accepted 30 March 2022; published 12 April 2022)

We present an experimental study of quantum diffusion of atomic hydrogen in solid H_2 films at temperatures below 1 K. The atoms are generated via electron impact dissociation by running a continuous rf discharge in helium gas above the H_2 film for long (up to 30 days) times. We are able to distinguish between the diffusion of the atoms moving towards each other followed by their recombination and the pure spatial diffusion driven by the density gradient. We found that in both cases the flux of phonons generated by the discharge above the surface of molecular film is essential to observe the slow diffusive motion. We obtained rates of pure spatial diffusion of H atoms in normal- H_2 (75% ortho, 25% para) films which were two orders of magnitude faster than those obtained from the H atom recombination, the quantity used in all previous work to characterize the mobility of H atoms in solid H_2 . We investigated the influence of the film thickness and its ortho-para composition on recombination and pure spatial diffusion. For thin enough films of $0.16 \mu\text{m}$ we observed complete diffusion of the H atoms through the entire film thickness. We observed peculiar behavior of the samples with ortho- H_2 ($o\text{-H}_2$) concentration below 5%. The recombination rate in these samples was an order of magnitude faster while the rate of spatial diffusion was somewhat slower than in films containing larger $o\text{-H}_2$ concentrations. The rate of production of H atoms in the low $o\text{-H}_2$ samples turned out to be an order of magnitude larger. We discuss possible explanations of these somewhat contradictory observations.

DOI: [10.1103/PhysRevB.105.144102](https://doi.org/10.1103/PhysRevB.105.144102)**I. INTRODUCTION**

Hydrogen is the lightest and simplest among the elements. Along with solid helium [1,2] and molecular hydrogen isotopes [3], hydrogen atoms embedded in solid H_2 represent a class of so-called quantum crystals, the only solid-state systems where atomic and molecular diffusion does not freeze-out even at temperatures below 1 K.

At low temperatures, atomic diffusion in quantum crystals proceeds via tunneling when an atom propagates through a periodic matrix potential [4,5]. Tunneling in this case is characterized by a certain band associated with the atomic zero-point energy. The ideal case of resonant tunneling when the potential perturbation is smaller than the tunneling bandwidth was staged and extensively studied in assemblies of cold atoms in optical traps [6–9]. For atoms in real crystals, the tunneling bandwidth is much smaller than the energy level mismatch caused by lattice imperfections, and the tunneling rate becomes highly susceptible to perturbations of the matrix potential. As a result, tunneling diffusion slows down

significantly near the crystal imperfections when the resonant tunneling regime is not effective anymore. The energy level mismatch caused by the lattice defects can be compensated by phonons. A similar regime of photon-assisted tunneling is also known for other tunneling systems such as quantum dots [10]. For quantum crystals at $T \simeq 1$ K, the diffusion rate acquires a characteristic linear dependence on temperature [4,5].

Helium atoms diffuse through the lattice by interchanging their positions with the adjacent atoms [11]. The diffusion rate of ^3He atoms in solid ^4He was estimated in a number of nuclear magnetic resonance (NMR) spin-echo measurements with a linear dependence of the diffusion rate on ^3He atom concentration at temperatures below 1 K [12].

Similar to helium solids, an even lighter atomic species, a hydrogen atom, embedded in solid H_2 remains mobile and diffuses through the lattice at temperatures below 1 K. Unlike diffusion of helium atoms in the solid heliums, the H atom diffusion in solid H_2 at $T < 1$ K proceeds through a repetition of the most elementary chemical reaction $\text{H} + \text{H}_2 = \text{H}_2 + \text{H}$ [13,14] when a single H atom interchanges position with

an H atom of the neighboring H_2 molecule without a vacancy formation. The diffusion of H atoms in solid H_2 is conventionally detected and probed through their recombination back to H_2 molecules using electron-spin resonance (ESR). In this process, two hydrogen atoms first approach each other to occupy neighboring lattice sites and then recombine. As a result, the H atom diffusion rates obtained in recombination measurements are biased by the slower H atom diffusion at small H-H distances and do not provide a pure tunneling rate when H atoms move through the H_2 matrix potential far from other unpaired hydrogen atoms. Due to a stronger van der Waals interaction and a completely different diffusion mechanism, the H atom diffusion in solid H_2 proceeds much slower [15] as compared with that of ^3He atoms in solid ^4He . This makes measurements of a pure H atom spatial diffusion in solid H_2 a much more challenging task.

The studies of H atom quantum diffusion in solid H_2 began in the 1980s when the recombination measurements [13,16–20] and the first attempts to measure the pure spatial diffusion [21] were carried out. These early studies made an important contribution to theoretical calculations of the $\text{H} + \text{H}_2 = \text{H}_2 + \text{H}$ reaction rates at ultralow reactant energies [22,23]. The later recombination studies of H atoms in solid H_2 provided insight into the role of ortho-para composition on the H atom recombination rate [24,25] and revealed a significant deviation of the H atom diffusion rate temperature dependence from the linear behavior predicted for $T < 1$ K [26,27].

Later studies utilized other approaches, such as H atom catalyzed ortho-para conversion in solid H_2 [28,29] and the rates of diffusion-limited chemical reactions of H atoms with simple organic and inorganic molecules [30–32]. These studies provided new and important information on quantum diffusion of H atoms but were unable to obtain the pure H atom spatial diffusion rates.

In our previous work [15], we carried out the first measurement of a pure H atom spatial diffusion in solid H_2 at $T = 0.7$ K. We made two different measurements of H atom diffusion in the same experiment: the one based on H atom recombination and the other on H atom diffusion based on their propagation into the film bulk. In our experiments, we stimulated the H atom diffusion with phonons created in the H_2 film by running an rf discharge above the top surface of our H_2 samples. We observed a two-order-of-magnitude faster pure H atom spatial diffusion rate as compared to that obtained from the H atom recombination.

In this work, we provide further insight by carrying out H atom diffusion measurements for H_2 films of different thicknesses and ortho-para content. We observed an order of magnitude higher accumulation rate of H atoms in para- H_2 ($p\text{-H}_2$) samples as compared to that in the H_2 films with an initial normal- H_2 ($n\text{-H}_2$) ortho-para content. In addition to that, we found out that the pure H atom spatial diffusion in $n\text{-H}_2$ samples proceeds slightly faster than in $p\text{-H}_2$ samples of the same thickness. For the thinnest films of $0.16 \mu\text{m}$ we observed complete diffusion of a high density front through the whole sample thickness reaching the substrate under the film. We propose possible explanations for the observed phenomena.

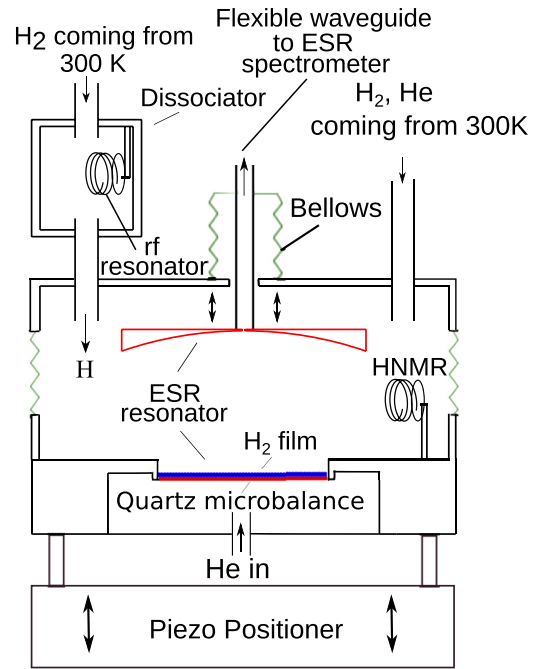


FIG. 1. Sample cell schematic.

II. EXPERIMENTAL SETUP

The experimental setup is based on a commercial Oxford 200 dilution refrigerator. The sample cell (SC) is attached to the refrigerator mixing chamber and also located at the center of a 4.6-T superconducting magnet [33] (Fig. 1). The main SC volume contains an open design Fabry-Perot resonator coupled to a 128-GHz electron spin resonance (ESR) spectrometer [34] through a waveguide assembly. The top spherical ESR resonator mirror is made of silver-plated polycrystalline copper, while the flat bottom gold-plated mirror also acts as the top electrode of a quartz microbalance (QM). We, therefore, simultaneously measured the H_2 film thickness by the QM and detected H atoms in the films by means of ESR.

We created the samples of H atoms in solid H_2 as follows. First, we deposited a solid hydrogen film onto the QM top electrode either directly from a room-temperature gas-handling system or we recondensed it from a specially arranged chamber, the dissociator, thermally insulated from the SC body by a stainless steel tubing assembly (see Fig. 1). In both cases, the H_2 films were deposited at a small rate of ≈ 1 monolayer/s for a substrate temperature of 0.5–1 K.

Normal composition molecular hydrogen was condensed into the dissociator at the beginning of the experimental run and kept there for the time of over 3 months during which four samples (samples 1, 3, 4, and 5 in Tables I and II) were created by redepositing the H_2 stored in the dissociator. Our estimates of the initial ortho-concentration after deposition are based on the natural conversion rate, as will be explained in details later. Due to the very slow deposition rate we were able to create polycrystalline molecular films with the high-homogeneity crystal field experienced by embedded H atoms, as verified by numerous previous experiments using ESR and ENDOR [27,35]. After creating the H_2 film, we kept the SC

TABLE I. Parameters for H atom diffusion obtained for n -H₂ samples and 95% p -H₂ (initial o - p composition) sample studied in this work and previous work (samples 1–3) [15] using a fitting function $x = x_0 + \sqrt{2D^d(t - t_0)}$. Here x_0 is the depth for creation of H atoms by direct dissociation of H₂ atoms by electron bombardment. t_0 is time when the H atom diffusion starts contributing to the propagation of the H atom rich layer into the H₂ film bulk. D^d is the pure spatial diffusion rate of H atoms into the H₂ film bulk. D_r^d is the diffusion rate associated with the H atom recombination. n is the maximum average local concentrations of H atoms obtained in the sample study. k is the constant H atom production rate due to the discharge. k_r^d is the recombination rate of H atoms.

Sample	1 [15]	2 [15]	3 [15]	7	8
Description	2.5 μm n -H ₂	2.5 μm n -H ₂	0.65 μm 95% p -H ₂	2.5 μm n -H ₂	0.16 μm n -H ₂
Symbols (in figures)	Red circles	Cyan triangles down	Magenta diamonds	Light-green asterisks	Brown stars
T (K)	0.67	0.67	0.67	0.6 (same discharge power)	
x_0 (nm)	80(20)	80(20)	80(20)	60(15)	60(15)
t_0 (h)	20(7)	20(7)	22(7)	42(14)	18(6)
D^d ($\times 10^{-16}$ cm ² s ⁻¹)	1.5(5)	1.5(5)	1.3(5)	1.7(6)	1.5(5)
D_r^d ($\times 10^{-18}$ cm ² s ⁻¹)	0.4(1)	0.3(1)	0.3(1)	0.3(1)	0.3(1)
n ($\times 10^{19}$ cm ⁻³)	1.3(1)	1.3(1)	1.4(1)	1.0(1)	1.2(1)
k ($\times 10^{14}$ cm ⁻³ s ⁻¹)	0.6(2)	0.5(2)	0.5(2)	0.3(1)	0.4(1)
k_r^d ($\times 10^{-25}$ cm ³ s ⁻¹)	1.8 (6)	1.5(5)	1.3(4)	0.9(4)	1.4(4)

temperature at $T = 0.7$ K, condensed about 5 μmole of helium gas into the SC, and started the rf discharge in the vicinity of the deposited H₂ films by applying short resonant rf pulses to the HNMR coil (Fig. 1).

We added helium gas to the sample cell with the main goal to create and maintain the discharge above the H₂ film for generation of H atoms in the film. At temperature 0.67 K the saturated vapor pressure of ⁴He gas is ~ 0.2 Pa, which allows us to start and maintain a stable discharge in helium gas in the sample cell. At temperature 0.6 K the saturation vapor pressure of ⁴He gas dropped to 0.02 Pa and we were not able to start the discharge in ⁴He gas at this temperature. Therefore, at $T = 0.6$ K we used a ³He - ⁴He gas mixture to run the discharge. The saturated vapor pressure of ³He gas at $T = 0.6$ K is 70 Pa allowing us to run and sustain the discharge. Another useful feature of the presence of ⁴He gas in the sample cell at these low temperatures is the formation of a ⁴He superfluid film on the surface of the H₂ film. Due to high thermal conductivity, the ⁴He superfluid film pro-

vides effective cooling of the H₂ film during action of the rf discharge.

The electrons created during the SC discharge bombarded the H₂ films and dissociated a fraction of hydrogen molecules there, thus giving rise to the number of H atoms in solid H₂ films which we detected by the ESR method. We ran the rf discharge in the SC continuously for all samples we discuss. This way continuous dissociation in the film provided a source of atoms with a constant rate over a long measurement time. In addition, a continuous flux of phonons in the films was generated, which facilitated a faster motion of the atoms in the H₂ crystals. Our previous attempts to observe pure spatial H atom diffusion without the phonon flux generated during the rf discharge appeared to be unsuccessful.

Along with the helical resonator in the SC, we also arranged a small rf resonator in the hydrogen dissociator chamber (Fig. 1). By running the rf discharge in the dissociator, we created a flux of atomic hydrogen gas into the SC volume. We used ESR spectra of gas-phase hydrogen atoms to

TABLE II. Parameters for H atom diffusion obtained for H₂ samples with initial p -H₂ content $\geq 97\%$ studied in this work using a fitting function $x = x_0 + \sqrt{2D^d(t - t_0)}$. Here x_0 is the depth for creation of H atoms by direct dissociation of H₂ atoms by electron bombardment. t_0 is time when the H atom diffusion starts contributing to the propagation of the H atom rich layer into the H₂ film bulk. D^d is the pure spatial diffusion rate of H atoms into the H₂ film bulk. D_r^d is the diffusion rate associated with the H atom recombination. n is the maximum average local concentrations of H atoms obtained in the sample study. k is the constant H atom production rate due to the discharge. k_r^d is the recombination rate of H atoms.

Sample	4	5	6
Description	0.2 μm 97% p -H ₂	0.65 μm 98% p -H ₂	2.5 μm 99.8% p -H ₂
Symbols (in figures)	Green triangles up	Black hexagons	Blue squares
T (K)	0.67	0.67 (low discharge power)	0.67
x_0 (nm)	90(20)	70(15)	130(30)
t_0 (h)	14(4)	47(15)	18(6)
D^d ($\times 10^{-17}$ cm ² s ⁻¹)	4(2)	3(2)	5(2)
D_r^d ($\times 10^{-18}$ cm ² s ⁻¹)	2.4(8)	0.9(3)	6(2)
n ($\times 10^{19}$ cm ⁻³)	2.0(1)	1.4(1)	1.3(1)
k ($\times 10^{14}$ cm ⁻³ s ⁻¹)	9(3)	1.7(6)	10(3)
k_r^d ($\times 10^{-25}$ cm ³ s ⁻¹)	11(4)	4 (1)	30(7)

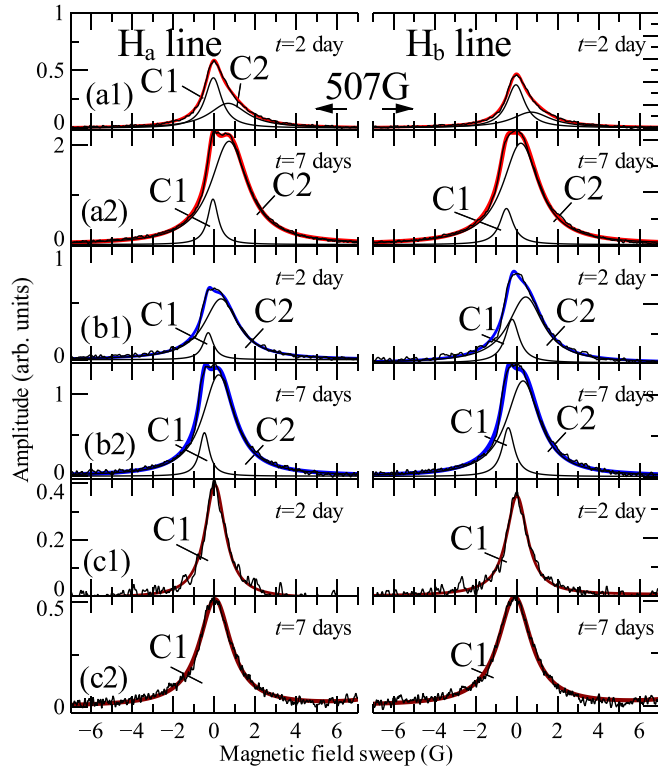


FIG. 2. ESR spectra of H atoms in solid H_2 for different samples: the low-field (H_a) and high-field (H_b) ESR lines of H atoms measured in 2.5- μm -thick $n\text{-H}_2$ sample 1 after 2 days (a1) and 7 days of running the discharge (a2), in 2.5- μm -thick $p\text{-H}_2$ sample 6 [(b1) and (b2), respectively], and in 0.16- μm -thick sample 8 [(c1) and (c2), respectively]. The line models used to fit the spectra measured for samples 1, 6, and 8 are shown with solid red, blue, and brown lines, respectively.

calibrate the areas under the ESR lines of H atoms in solid H_2 to find an absolute number of H atoms in the solid hydrogen films we studied [15].

The ESR spectrum of atomic hydrogen consists of two lines separated by 507 G in the experimental field of 4.6 T (Fig. 2). We sweep magnetic field in the vicinity of these two transitions to resolve their shapes and structures as well as integrals and widths. The widths of H atom ESR lines at high densities are determined mostly by a concentration-dependent contribution from the dipole interaction between electron spins [27,36]. We use this broadening effect for evaluation of the average density of H atoms. ESR line integrals are in turn proportional to the total number of H atoms in the films. As we observed in our previous work and present here, diffusion of atoms leads to an appearance of two regions along the film thickness with high and low local concentration of atoms. This is seen as a double-peak structure of ESR lines. Making double fit of the ESR lines we evaluate local densities in these regions via the above-mentioned dipolar broadening effect. For most of the spectra presented here, the contribution of the low-density region can be neglected and it is sufficient to plot an average density evaluated from the Lorentzian fit of the ESR line. Using a total number of atoms extracted from

the ESR line integrals we evaluate the effective depth of the H-rich layer and measure its evolution during experiment.

III. EXPERIMENTAL RESULTS

In this work, we investigated the factors that might affect the pure spatial H atom diffusion in solid H_2 first studied in our previous work [15]. We analyzed the influence of initial ortho-para content, H_2 film thickness, H atom concentration, and the rf discharge power on H atom diffusion. We included in this paper the results of investigations of three previously studied H_2 samples [15]: 2.5 μm normal- H_2 (75% ortho, 25% para) films (samples 1 and 2) and a 0.65- μm thick $n\text{-H}_2$ film (sample 3) prepared from $n\text{-H}_2$ gas stored in the dissociator for 40 days, so we estimated the initial $p\text{-H}_2$ fraction in the film to be $\approx 95\%$ considering an $o\text{-}p$ natural conversion rate $K = 0.019 \text{ h}^{-1}$ [37]. In addition, the following samples were prepared and studied to complement our earlier results. Sample 4 was a 0.2- μm -thick H_2 film made from H_2 stored in the dissociator chamber for two months. For this sample, we estimated that initial ortho-para content was reduced from 75% to about 3% (97% para) by natural ortho-para conversion [37]. Sample 5 was a 0.65- μm -thick film made of H_2 gas with 98% $p\text{-H}_2$ fraction. Sample 6 was a 2.5- μm thick $p\text{-H}_2$ film which was made from H_2 converted in an ortho-para converter filled with $\text{Fe}(\text{OH})_3$ powder [38] and stored at 20 K for about 1 day. This ensures conversion of the initial gas to about 99.8% $p\text{-H}_2$ since the time constant for ortho-para ($o\text{-}p$) conversion in the presence of paramagnetic salts is of order seconds to minutes [37]. Sample 7 was a 2.5- μm $n\text{-H}_2$ film. Finally, sample 8 was a 0.16- μm -thick $n\text{-H}_2$ film. We used the same discharge parameters and rf power for samples 1, 2, 3, 4, 6, and 8 keeping the sample cell temperature at $T = 0.67 \text{ K}$. We ran the discharge for sample 5 at a three times lower power, but stabilized the SC temperature at 0.67 K using an electrical heater. The H atom accumulation in sample 7 was carried out by running the rf discharge using the same discharge power as for samples 1–4, 6, and 8, but instead of pure ^4He , we condensed 10 μm of a $^3\text{He}\text{-}^4\text{He}$ mixture to be able to sustain the rf discharge at a lower temperature $T = 0.6 \text{ K}$. We summarize the description of samples 1, 2, 3, 7, 8 with estimated initial $o\text{-H}_2$ content $\geq 5\%$ in Table I. The description of samples 4, 5, and 6 with initial $o\text{-H}_2$ content $\leq 3\%$ is presented in Table II.

To our knowledge, the rate of natural $o\text{-}p$ conversion in solid H_2 was not measured at temperatures below 1 K. Therefore, our estimates for ortho-para content in the H_2 samples 3, 4, and 5 are based on the values obtained at temperatures $\geq 1.57 \text{ K}$ [39,40]. Faster natural $o\text{-}p$ conversion at lower $o\text{-H}_2$ concentrations [40], as well as slower $o\text{-H}_2$ molecule diffusion and the effects of $o\text{-H}_2$ molecule clustering, can cause a deviation from our estimates of the initial $o\text{-}p$ concentrations in these samples. Thus, the values of the initial $o\text{-H}_2$ concentration presented for the samples created with molecular H_2 kept for a long time in the dissociator are actually conservative upper limit estimates of the real concentration.

We found that the H atom accumulation during the discharge consisted of two distinct stages. During the first stage, that lasted less than one day in $p\text{-H}_2$ samples 4 and 6 and about four days in the $n\text{-H}_2$ samples, the H atom linewidth increased

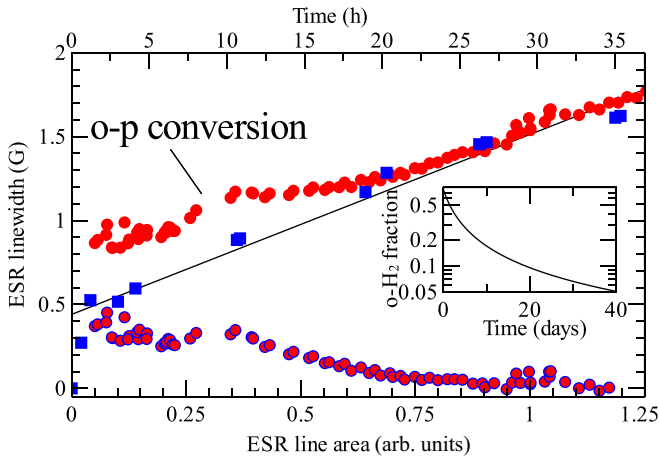


FIG. 3. Dependence of ESR linewidth on ESR line area at the beginning of accumulation for n -H₂ sample 1 (red circles) and p -H₂ sample 6 (blue squares). The timescale applies to sample 1 only. An extra o -H₂ H atom ESR line broadening in sample 1 estimated as a difference between the red points of sample 1 and the solid fitting line is presented by red/blue circles. An estimated o -H₂ fraction evolution in n -H₂ samples due to natural o - p conversion is presented in the figure inset [37].

proportionally to the ESR line integrals. A characteristic feature of the first accumulation stage is a gradual linear increase of the average H atom concentration proportionally to the number of H atoms in the H₂ film. In this regime, the ESR lines of H atoms in 2.5, 0.65- μ m-thick films had a composite shape and consisted of two components: a narrow component (C1) and a broader component (C2) [see Figs. 2(a1) and 2(a2) and 2(b1) and 2(b2)]. These two components can be assigned to two regions of different local H atom concentration regardless of their initial ortho-para composition.

During the second stage of accumulation, the ESR linewidth of both components did not change even though the total number of H atoms continued to grow. We observed the development of a clear ESR line asymmetry and an increase of the broad C2 component similar to our previous work [15,41]. The intensity of the narrow C1 component did not change during the second accumulation stage. Unlike the thicker samples, we did not observe asymmetry in the ESR lines of H atoms in 0.16- μ m-thick n -H₂ sample 8. For the sample 4 with a 0.2- μ m thickness such asymmetry was barely resolved. These lines remained Lorentzian during the whole time of running the rf discharge [Figs. 2(c1) and 2(c2)].

The ESR lines were broadened by the dipolar interaction between the H atom electron spins in both p -H₂ and n -H₂ samples but had an extra contribution due to hyperfine interaction of H atom electron spins with nuclei of o -H₂ molecules in the n -H₂ films at the beginning of accumulation. For the n -H₂ samples 1, 2, 7, and 8 in the very beginning of sample accumulation, we observed an additional ESR line broadening caused by neighboring o -H₂ molecules. This o -H₂ contribution decreased gradually and vanished nearly completely after about 25 hours of accumulation (Fig. 3). We present time evolution of the estimated broadening of H atom ESR lines in sample 1 due to o -H₂ molecules with blue-red circles. Natural o - p conversion in solid H₂ is a two-body process which proceeds

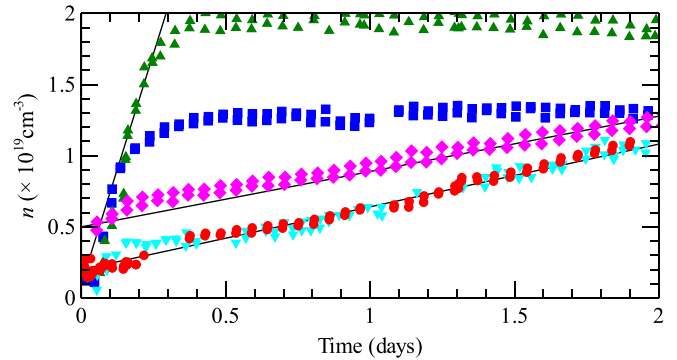


FIG. 4. Evolution of H atom average concentration n during first two days of running the rf discharge in samples 1 (red circles), 2 (cyan triangles down), 3 (magenta diamonds), 4 (green triangles up), and 6 (blue squares). The slopes of solid lines provide estimates for the H atom production rates k .

with a rate of $\simeq 1.9\%/h$ [37]. The presence of H atoms in H₂ films enhances the o - p conversion rate of H₂ molecules in the vicinity of these atoms [28]. We present an estimate of o -H₂ fraction evolution in n -H₂ due to natural conversion in the inset of Fig. 3.

In the course of running the SC discharge, we also observed an unexpectedly high-production efficiency of H atoms in p -H₂ sample 6 and 97% p -H₂ sample 4. The production rate of H atoms in these samples was about one order of magnitude higher than in the samples made of H₂ gas of a natural ortho-para composition (Fig. 4 and Tables I and II). The accumulation rate in sample 3 (95% para-H₂) was similar to the rate for samples with a normal o -H₂ content. The accumulation rate in sample 5 (98% para-H₂) where we used a three times lower discharge power was about three times higher than in n -H₂ samples, but about five times below that in p -H₂ samples 4 (97% para-H₂) and 6 (99.8% para-H₂).

Despite a much higher H atom production rate, the maximum average H atom concentrations in p -H₂ samples 4 and 6 did not exceed those observed for the n -H₂ samples [see Fig. 5(a)] and reached a value of $1\text{--}2 \times 10^{19} \text{ cm}^{-3}$. The final H atom concentrations saturated in half a day for the p -H₂ samples and about four days for the n -H₂ films. Time evolution of the average local concentrations and total number of H atoms in samples 1–7 is presented in Figs. 5(a) and 5(b).

In the Figs. 5(a), 6(a), and 7(a) we present average local concentrations of H atoms which were calculated as weighted contributions from the two ESR line components. Since the C2 component areas significantly exceeded those of C1 after a few days of running the discharge [Figs. 2(a)–2(c), and 7(a) and 7(b)], we found that a single Lorentzian fit is a simple and accurate way to determine and present the weighted average concentrations of H atoms. In this case, they are almost completely defined by the C2 while C1 components contributed only to a small deviation from the Lorentzian line shape.

Similar to our previous work [15], we observed that the total number of H atoms in samples 1–6 continued to increase even when the average local concentrations of H atoms saturated [see Figs. 5(b), 6(b), and 7(b)]. Running the SC discharge for 0.16- μ m-thick sample 8 led to saturation of the H atom concentration after about 4 days [Fig. 6(a)] and

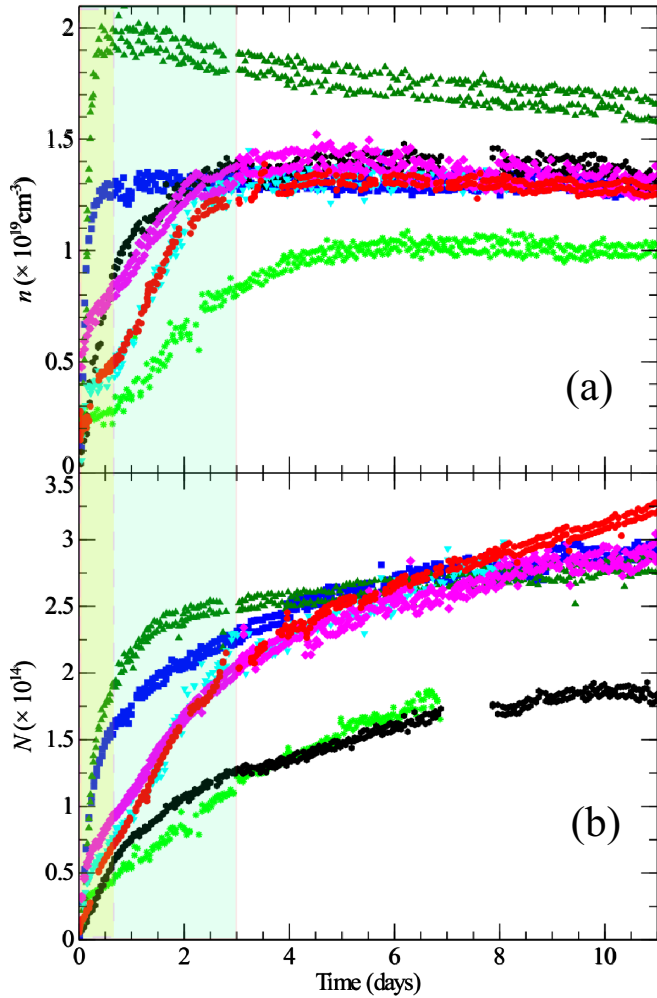


FIG. 5. (a) Time evolution of H atom concentration n in solid H_2 sample obtained from linewidth as discussed in this work: sample 1 (red circles), 2 (cyan triangles down), 3 (magenta diamonds), 4 (green triangles up), 5 (black hexagons), 6 (blue squares), 7 (light green asterisks) (b) Time evolution of the total number of atoms N in the same samples as in (a). The first accumulation stage characterized by saturation of H atom concentration for p - and n - H_2 samples is shown with pale yellow and green large background rectangles, respectively. The absence of points in (b) for sample 7 (light-green asterisks) is due to an ESR signal amplitude instability at 6 days $< t < 13$ days that did not, however, influence the linewidth analysis needed for finding n .

the total number of H atoms [Fig. 6(b)] in this sample after about 9 days. Neither the total number of H atoms nor local concentration changed after running the SC discharge for 6 more days.

We carried out an ESR line area calibration after studying every sample discussed above. First, we ran the rf discharge in the dissociator chamber to create a flux of H-gas atoms into the SC. After accumulating H-gas atoms in the SC, we induced their recombination and then calculated a correspondence between the recombination heat released and the decrease of the area under the gas-phase H atom ESR line which is proportional to the number of recombined atoms. Finally, we were able to calibrate the ESR line area for H

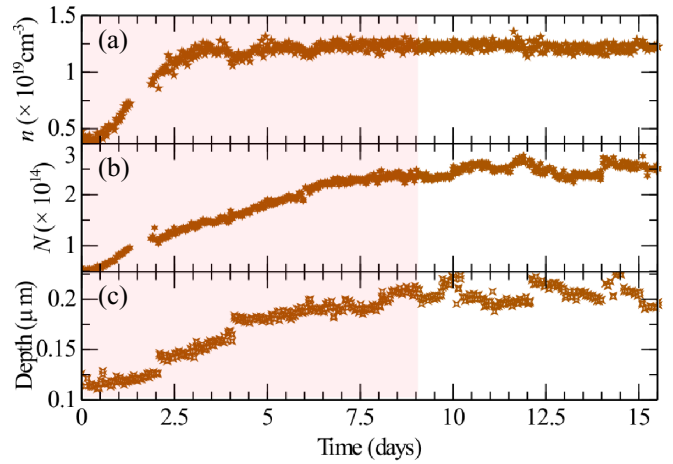


FIG. 6. Time evolution of H atom concentration n (a), total number of H atoms N (b), and the depth of H atom concentrated region obtained for sample 8 (c). The stage of filling the H_2 film with H atoms is shaded pink. A time period when the H atoms reached the substrate (QM) corresponds to the white area.

atoms in solid H_2 by comparing the resonator filling factors for H atoms in the gas phase and in the H_2 films (see Supplemental Material of Ref. [15]). We ran several calibration sequences and used an average value for the further analysis. We consider the calibration error to be about 30%.

A. Diffusion rate analysis

Previously, we observed a composite two-component structure of H atom ESR lines in μm -thick H_2 films [15,41]. In this work, we also studied 0.16- and 0.2- μm -thick films. We did not observe a clear deviation from the Lorentzian line shape for the 0.16- μm sample 8 during the entire sample

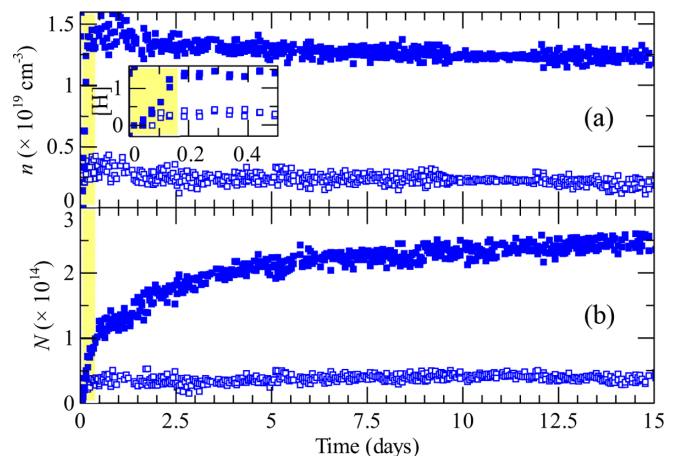


FIG. 7. Time evolution of the local concentrations n (a) and number (b) of H atoms N corresponding to components C1 (open blue squares) and C2 (filled blue squares) measured in sample 6. The inset in (a) presents the evolution of local concentrations of H atoms in sample 6 during the first half day of running the SC discharge. The units used in the inset are the same as in the main figure. The accumulation stage 1 as described in the text is shown by yellow rectangles.

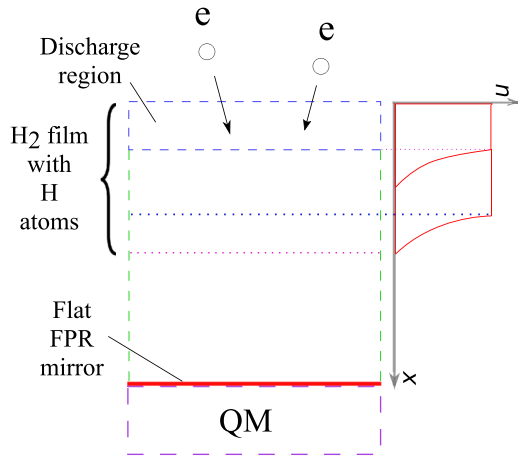


FIG. 8. Schematic representations for propagation of two sample regions of a high and low H atom local concentration n into an H_2 film after the formation of the H atom high-concentration layer. The total H_2 film thickness is designated as x .

accumulation. For slightly thicker sample 4 small double-peak structure was barely resolved. Similar ESR line shapes with simple one-component were also observed for H atoms in 2.5- μm -thick H_2 films bombarded by 5.7-keV electrons created during tritium decay [42]. We calculated that the ≈ 100 eV electrons generated during the rf discharge were able to penetrate into the H_2 film within about 100 nm [35]. The high-energy electrons released during tritium decay pierced the entire film and dissociated hydrogen molecules uniformly without creating an H atom concentration gradient. These observations support our assignment for the two ESR line components: a high-concentration surface layer corresponding to the broader component (C2) and the narrow component (C1) corresponding to the H atom low-concentration region at the front of a propagating H atom rich surface layer (see Fig. 8).

In this and previous work, we observed two distinct stages of H atom accumulation. During the first stage, the first 1–2 days of running the discharge, the H atom local concentration increased linearly and proportionally to the total number of H atoms. During the second stage, running the discharge further the average local H atom concentrations did not increase anymore even though the total number of H atoms in the H_2 films continued to grow steadily as shown in Figs. 5(a) and 5(b). Based on the ESR component widths, we estimated the local concentration of H atoms corresponding to components C1 and C2 as $\approx 5 \times 10^{18}$ and $1.5\text{--}2 \times 10^{19} \text{ cm}^{-3}$, respectively, for the samples we studied. As an example, we present time evolution of local concentrations and number of H atoms corresponding to both components in sample 6 in Figs. 7(a) and 7(b), respectively. As described earlier, the very small contribution from C1 allowed us to use weighted average concentrations for analyzing and presenting the experimental data.

During the second accumulation stage, the local concentrations corresponding to both components stopped changing within the accuracy of our fits [see Fig. 7(a)]. The total number of H atoms corresponding to the narrow C1 component remained constant, whereas the total number of H atoms form-

ing the broader component C2 continued to grow steadily. This observation led us to a conclusion that the diffusion can be considered as a propagation of a high-concentration layer front deeper into the H_2 film. The schematic representation of this process is shown in Fig. 8. An instantaneous H atom concentration in the H_2 films, $n(t)$, can be calculated by solving a differential equation

$$dn/dt = k - 2k_r^d n^2(x, t) - D^d d^2n/dx^2, \quad (1)$$

where k is the constant H atom production rate due to the discharge, k_r^d is a recombination rate of H atoms, and D^d is a pure spatial diffusion rate of H atoms into the bulk, where x is the thickness of the H atom rich layer, respectively. We calculated production rates k by analyzing the beginning of the first accumulation stage when the H atom concentration was small enough ($n_H < 5 \times 10^{18} \text{ cm}^{-3}$) and increased linearly with time, so the contribution from the recombination and diffusion terms to the H atom concentration change was still insignificant. At the end of the first stage when $dn/dt = 0$ and the diffusion contribution is still small, the production and recombination terms become equal, leading to the equilibrium concentration

$$n_{eq} = \sqrt{k/2k_r^d} \quad (2)$$

that was approached with a characteristic time $\tau = 1/\sqrt{2kk_r^d}$ [43]. From Eq. (2) we calculated the recombination rates as $k_r^d = k/2n_{eq}^2$ (Tables I and II). The diffusion rate D_r^d associated with the H atom recombination can be calculated from measured values of k_r^d by using a relation $D_r^d = k_r^d/4\pi a_0$, where $a_0 = 3.78 \text{ \AA}$ is the lattice constant of solid H_2 .

During the second accumulation stage, the diffusion term became responsible for a gradual increase of the number of H atoms even though the H atom concentration in the layer stopped changing. We did not observe narrowing of the C2 component or increase of C1 as might be expected upon formation of the vertical H atom concentration gradient according to the term $D^d d^2n/dx^2$ of Eq. (1). Since only the intensity of their broad component increased during continuously running the discharge, we concluded that no H atom concentration gradient appeared within the H atom rich layer corresponding to C2. As a result, the front of this layer first created close to the sample surface propagates deeper into the film bulk with a rate determined by the pure spatial diffusion D^d . The pure spatial diffusion rate can be calculated by solving differential Eq. (1). In our work, we implemented a simplified approach to finding the pure spatial diffusion rate of H atoms. We calculated the H atom penetration depth into the film bulk using a total number of H atoms obtained from the ESR line area calibration, the local H atom concentration estimated from the ESR linewidth of H atoms in solid H_2 , and the known surface area of the H_2 film grown on the QM. We consider that the distance the H atoms at a front of the rich layer diffuse into the film bulk x can then be found from the solution of Fick's diffusion law for a one-dimensional case. We tested several fitting models able to describe the propagation of H atom rich layer into the film bulk. We fit the experimental data presented in Fig. 9 with square-root

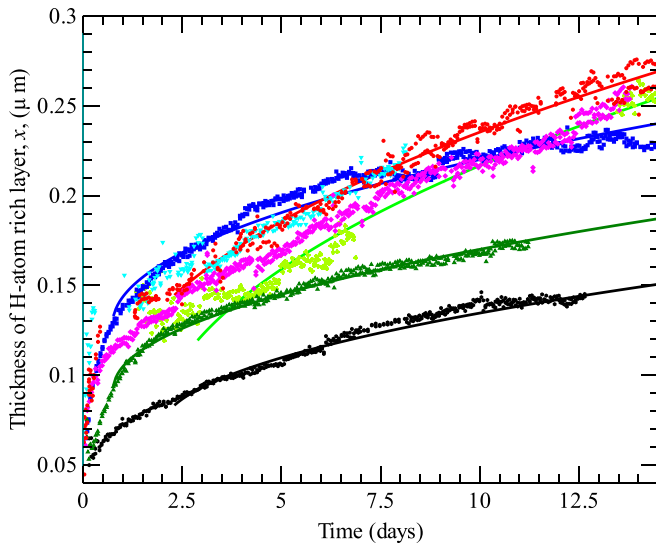


FIG. 9. Dependence of the H atom rich layer thickness on time showing the H atom diffusion in sample 1 (red circles), sample 2 (cyan triangles down), sample 3 (magenta diamonds), sample 4 (green triangles up), sample 5 (black hexagons), sample 6 (blue squares), sample 7 (light-green asterisks). Solid lines show a square-root fit according to Eq. (3).

functions according to Eq. (3):

$$x = x_0 + \sqrt{2D^d(t - t_0)}. \quad (3)$$

Here x_0 describe the thickness of highly concentrated layer of H atoms in the H_2 films formed by direct dissociation due to electron bombardment. The values obtained, $x_0 \simeq 100$ nm, agree with our estimates for the penetration depth of electrons created during the rf discharge in our experiments [35]. t_0 is the time for the formation of the initial highly concentrated layer after which the H atom diffusion starts contributing to the propagation of H atom rich layer into the H_2 film bulk. We also found that variation of both x_0 and t_0 changes the values of D^d within about 20%.

We also append the values for spatial diffusion reported in our previous work [33] for samples 1–3 based on this model. The obtained fitting parameters are presented in Tables I and II. The fits presented in Fig. 9 cover the points corresponding to the second accumulation stage when only the pure spatial diffusion leads to increase of the H atom rich layer thickness x .

In sample 8 we were able to observe a propagation of the high-concentration layer through the whole volume of the thin $0.16\text{-}\mu\text{m}$ H_2 film. In this sample, both the H atom concentration n and the number of atoms N leveled off [Figs. 6(a) and 6(b)]. We made an estimate of the H atom rich level thickness $x \simeq 0.20(2)\ \mu\text{m}$ [Fig. 6(c)]. This value is about 25% greater than the H_2 film thickness measured by the QM ($0.16\ \mu\text{m}$) during the film deposition. We note that this value lies within the uncertainty of our ESR line area calibration which is about 30%.

IV. DISCUSSION

We carried out a series of studies of the H atom pure spatial and recombination diffusion in H_2 films of different thicknesses (2.5 , 0.65 , and $\simeq 0.2\ \mu\text{m}$) and different ortho- H_2 content (normal- and para- H_2 films) and at temperatures $T = 0.67$ and 0.6 K. The investigations of spatial diffusion in $n\text{-}H_2$ do not show any dependence of diffusion coefficient on the H_2 film thickness in the range $0.16\text{--}2.5\ \mu\text{m}$. For all samples in accordance with our previous publication [15], spatial diffusion of H atoms was more than two orders of magnitude faster than that obtained from recombination rate of H atoms (see Table I). A similar result was obtained for sample 3 with 95% of $p\text{-}H_2$. Investigations of spatial diffusion in the samples with high initial contents of $p\text{-}H_2$ (95%–99%) show rather different results (see Table II and sample 3 in Table I). Decreasing content of $o\text{-}H_2$ molecules below 3% led to some unusual effects. The coefficient of spatial diffusion for H atoms in these samples became smaller than that for the $n\text{-}H_2$ films, while the recombination diffusion of H atoms in these samples increased by an order of magnitude as compared to that observed for $n\text{-}H_2$ samples. Moreover, the values of D^d obtained for samples with small initial content of $o\text{-}H_2$ (samples 3 and 4) show a strong influence of $o\text{-}H_2$ molecules on the process of spatial diffusion in $n\text{-}H_2$ samples. As a result, for samples studied with a small initial concentration of $o\text{-}H_2$ molecules ($\leq 3\%$), the spatial diffusion is also faster than that obtained for recombination of H atoms in these samples, but this difference is only one order of magnitude. This is probably a result of a larger recombination diffusion rate of H atoms in these samples.

Another effect observed in this work is a fast accumulation rate of H atoms in the $p\text{-}H_2$ samples which is one order of magnitude higher than that for the accumulation rate of H atoms in $n\text{-}H_2$ samples. At the same time, the maximum concentration of H atoms achieved in both $n\text{-}H_2$ and $p\text{-}H_2$ samples was very similar, of order $(1.1\text{--}2) \times 10^{19}\text{cm}^{-3}$.

We now consider possible explanations for these effects. First, we discuss a higher production rate of H atoms in 98% $p\text{-}H_2$ sample 4 and 99.8% $p\text{-}H_2$ sample 6 (see Fig. 4 and Tables I and II) which exceeded that in the $n\text{-}H_2$ samples 1, 2, 7, 8 and a 95% $p\text{-}H_2$ sample 3 by about an order of magnitude. We did not observe any change of production rate k due to the process of continuing stimulated and natural $o\text{-}p$ conversion of H_2 molecules which significantly decreased $o\text{-}H_2$ content in the films during this time interval (Fig. 3).

In our previous work on studying H atoms in solid H_2 where H atoms were created by exposing solid H_2 films to a flux of 5.7 keV electrons released during tritium decay [44], we also observed a higher production rate for H atoms in $p\text{-}H_2$ stored at $T = 0.15$ K. Unlike this work where the discharge produced H atoms in the surface layers $\simeq 100$ nm, high-energy electrons in the former study dissociated H_2 molecules in the $2.5\text{-}\mu\text{m}$ -thick films uniformly. As a result, the H atom diffusion in the film was limited to the mean interatomic distances ~ 10 nm. We, therefore, suggest that a more efficient diffusion of H atoms into the bulk in $n\text{-}H_2$ samples cannot explain faster accumulation of H atoms in $p\text{-}H_2$ samples observed in this work. An independence of the production rate on time in this work within the first 1–2 days of

running the discharge also excludes the possibility for different cross sections of p -H₂ and o -H₂ molecular dissociation as well as different penetration depths of the discharge electrons into the films. Another possibility for a larger production rate of H atoms in solid p -H₂ might be a slower vibrational relaxation of excited H₂ molecules. In this case, an H₂ molecule in p -H₂ environment after collision with an electron is excited to the dissociation threshold and due to a longer vibrational relaxation time may have a higher probability to split into two H atoms instead of relaxing back to the ground vibrational state.

Kumada *et al.* [25] studied the recombination behavior of H atoms in solid H₂ of different ortho-para composition at $T = 4.2$ K and reported a striking dependence of the H atom recombination rate k_r on ortho-H₂ concentration with a k_r maximum at $C(\text{ortho}) \simeq 8\%$. Smaller k_r of H atoms in H₂ with o -H₂ admixtures below $\simeq 8\%$ was explained by a possible smaller probability for recombination of two H atoms in the neighboring lattice sites in pure p -H₂. The authors suggested [25] that the presence of o -H₂ molecules with a nonzero quadrupole moment in the vicinity of an excited H₂ molecule may activate vibrational deexcitation associated with infrared emission. This pathway is prohibited in a pure p -H₂ crystal [45] but can be activated by small o -H₂ admixtures of order 1%. The relaxation of vibrationally excited H₂ molecules in solid H₂ was measured up to $v = 3$ vibrational level at $T \approx 11$ K and did not show a difference in H₂ molecule vibrational relaxation times for para- and normal-H₂ samples (both are of order μs) [46]. Therefore, the observed phenomena of different production rates in n -H₂ and p -H₂ cannot be explained by different vibrational relaxation rates of p -H₂ and o -H₂ molecules.

Since the production of H atoms during the first stage of running the discharge is a random process, H atom pairs generated during dissociation in an o -H₂ rich environment can temporarily become trapped there due to a higher energy level mismatch and, thus, have a higher probability of recombining back. On the other hand, H atom recombination in an o -H₂ molecule rich matrix is also less efficient (see Tables I and II). Nearly equal steady-state concentrations of H atoms in all samples we studied may indicate that the ortho-para content in the H atom rich regions became the same for both these types of samples during the second stage of running the discharge corresponding to the increasing size of the high H atom concentration region. Further studies may provide more insight into this phenomenon.

Second, we discuss observed differences in the spatial diffusion rate in H₂ films with different contents of ortho-H₂ molecules. Intensive studies of the properties of H₂ solids at small concentrations of o -H₂ were performed by NMR (see review by Meyer [47]). They revealed rearrangement of the normal distribution of ortho-molecules and formation of clusters of o -H₂ is a result of quantum diffusion in the temperature range down to 20 mK [48]. It turned out that the interactions between o -H₂ molecules of the pairs facilitate a faster conversion rate [40]. Enhancement of the conversion rate is also caused by a presence of other paramagnetic impurities: O₂ or H atoms [49]. A presence of free electrons in our H₂ films upon running the discharge should bring an extra conversion mechanism. Therefore, the values of the

ortho-concentration presented for our samples provide only a rough idea of the initial conditions. One may expect that quite rapidly the o -H₂ concentration reaches values substantially smaller than those at the start of the discharge, and all our samples with initial o -H₂ concentration $< 5\%$ should become nearly pure para-H₂ already after few hours. However, we see drastic difference in the properties of sample 3 from the rest of the para-rich H₂ samples with smaller than 5% initial concentration. This observation suggests that this difference appears at the initial stage, during deposition of the molecular films.

It is known that below 1 K, solid molecular hydrogen undergoes a phase transition from the fcc to hcp lattice at o -H₂ concentrations around 55% [50]. In the case of thin films studied in this work, one may expect that due to the influence of the substrate, different lattice structures are formed for samples with o -H₂ concentration as low as 5%. Quantum diffusion of H atoms in the lattice of H₂ may depend on the direction of the tunneling motion in the crystal. An anisotropy of the diffusion of o -H₂ impurities in the hcp lattice was observed in the NMR studies of this system [48]. For the diffusion of H atoms in our films, it may turn out that in high-purity p -H₂ crystals diffusion parallel to the surface of the film is substantially faster than that in the direction perpendicular to the film. This will lead to a faster recombination and larger k_r , as we observed for all samples with o -H₂ concentration below 5%. A factor of 2 smaller diffusion coefficients in the perpendicular to the surface direction found for these samples may be explained by different types of the lattice than in the samples with larger o -H₂ concentrations.

Furthermore, higher H atom mobility in a pure p -H₂ environment may also explain the faster accumulation rates k , for samples 4 (97% p) and 6 (99.8% p). In a uniform p -H₂ matrix, two H atoms produced after the H₂ molecule dissociation by electron impact have a higher probability to move apart from each other without recombining back and forming an H₂ molecule as compared with a more distorted matrix with a high o -H₂ content. Higher mobility of H atoms in a p -H₂ matrix free of o -H₂ impurities also promotes their faster recombination. The H atom production rate term k in Eq. (1) dominates when the recombination term is small, and the recombination term compensates it at higher H atom concentrations.

The samples we studied in this work had H atom concentrations of order $1.5 \times 10^{19} \text{ cm}^{-3}$. We observed the lowest diffusion rate for sample 4 with the highest average H atom concentration obtained, $2 \times 10^{19} \text{ cm}^{-3}$. On the contrary, the highest diffusion rate was observed in sample 7 with the smaller value of the maximum average local concentration of $\simeq 1 \times 10^{19} \text{ cm}^{-3}$. Despite large error margins, these observations may serve as preliminary evidence for H atom self-localization similar to that for ³He atoms in solid ⁴He [12] and H atoms in solid H₂ without running the discharge [27] in a comparable period of time. However, unlike solid helium mixtures where the ³He admixture can be easily controlled, we were unable to find steady-state conditions for studying pure spatial diffusion of H atoms in solid H₂ while running a discharge able to sustain the H atom concentrations $\sim 10^{18}$ or below. We will continue to search for such a regime in our future studies.

A presence of the continuous flux of phonons resulting from the discharge is important for accelerating the recombination and diffusion in the samples. As we pointed out, no spatial diffusion could be detected without running the discharge. The H atom recombination clearly slowed down (see Tables I and II) for a low-discharge power sample 5 as compared with sample 6. This effect, however, may have different strength in the samples with different *o*-H₂ concentrations. Remaining ortho-impurities move towards each other and form pairs or clusters with the characteristic time of the order of 10 h with the clusterization rate having a fairly flat maximum at around 0.3 K [48]. The *o*-H₂ clusters may absorb and emit phonons and also scatter them. These effects lead to a decrease of the phonon mean-free path and increase the time which they spend in the film before reaching the substrate. This increases probability of atomic jumps induced by the phonons and facilitates faster diffusion observed in this work.

V. CONCLUSION

In conclusion, we carried out a study of H atom diffusion in solid H₂ at $T = 0.67$ and 0.6 K in H₂ films with different

thicknesses (0.16 – 2.5 μm) and different ortho-H₂ content. The H atom diffusion was stimulated by phonons created in the H₂ film by running the rf discharge above the sample. In all H₂ we studied, the pure spatial H atom diffusion was one to two orders of magnitude faster than the diffusion obtained from the recombination rate of H atoms. In the latter case, the energy level mismatch impedes tunneling motion at small distances. We observed an order of magnitude faster accumulation rate of H atoms in para-H₂ samples as compared with the samples prepared from *n*-H₂. The difference in accumulation rates for H atoms in normal- and para-H₂ films cannot be explained by a more efficient vibrational relaxation of excited H₂ molecules in *n*-H₂ samples. We suggest a higher H atom mobility in pure *p*-H₂ samples may result in the higher H atom accumulation rate and their faster recombination. Additional experimental and theoretical efforts are needed for explaining this phenomenon.

ACKNOWLEDGMENTS

This work has been supported by NSF Grant No. DMR 2104756 and Academy of Finland Grant No. 317141.

-
- [1] N. Sullivan, *Prog. Nucl. Mag. Res. Sp.* **90-91**, 74 (2015).
- [2] C. Huan, L. Yin, J. S. Xia, D. Candela, B. P. Cowan, and N. S. Sullivan, *Phys. Rev. B* **95**, 104107 (2017).
- [3] D. Zhou, C. M. Edwards, and N. S. Sullivan, *Phys. Rev. Lett.* **62**, 1528 (1989).
- [4] Y. Kagan and L. A. Maksimov, *ZhETF* **44**, 459 (1983) [*Sov. Phys.-JETP* **57**, 459 (1983)].
- [5] Y. Kagan, *J. Low Temp. Phys.* **87**, 525 (1992).
- [6] H. Lignier, C. Sias, D. Ciampini, Y. Singh, A. Zenesini, O. Morsch, and E. Arimondo, *Phys. Rev. Lett.* **99**, 220403 (2007).
- [7] C. Sias, A. Zenesini, H. Lignier, S. Wimberger, D. Ciampini, O. Morsch, and E. Arimondo, *Phys. Rev. Lett.* **98**, 120403 (2007).
- [8] C. Sias, H. Lignier, Y. P. Singh, A. Zenesini, D. Ciampini, O. Morsch, and E. Arimondo, *Phys. Rev. Lett.* **100**, 040404 (2008).
- [9] A. Zenesini, C. Sias, H. Lignier, Y. Singh, D. Ciampini, O. Morsch, R. Mannella, E. Arimondo, A. Tomadin, and S. Wimberger, *New J. Phys.* **10**, 053038 (2008).
- [10] L. P. Kouwenhoven, S. Jauhar, K. McCormick, D. Dixon, P. L. McEuen, Y. V. Nazarov, N. C. van der Vaart, and C. T. Foxon, *Phys. Rev. B* **50**, 2019 (1994).
- [11] D. D. Osheroff, M. C. Cross, and D. S. Fisher, *Phys. Rev. Lett.* **44**, 792 (1980).
- [12] V. N. Grigor'ev, *Low Temp. Phys.* **23**, 3 (1997).
- [13] T. Miyazaki, K. P. Lee, K. Fueki, and A. Takeuchi, *J. Phys. Chem.* **88**, 4959 (1984).
- [14] T. Kumada, *Phys. Rev. B* **68**, 052301 (2003).
- [15] S. Sheludiakov, D. M. Lee, V. V. Khmelenko, J. Järvinen, J. Ahokas, and S. Vasiliev, *Phys. Rev. Lett.* **126**, 195301 (2021).
- [16] A. Y. Katunin, I. I. Lukashevich, S. T. Orozmatov, V. V. Sklyarevskii, V. V. Suraev, V. V. Filippov, N. I. Filippov, and V. A. Shevtsov, *Pis'ma Zh. Eksp. Teor. Fiz.* **34**, 375 (1981) [*JETP Lett.* **34**, 357 (1981)].
- [17] A. V. Ivliev, A. Y. Katunin, I. I. Lukashevich, V. V. Sklyarevskii, V. V. Suraev, V. V. Filippov, N. I. Filippov, and V. A. Shevtsov, *Pis'ma Zh. Eksp. Teor. Fiz.* **36**, 391 (1982) [*JETP Lett.* **36**, 472 (1982)].
- [18] A. V. Ivliev, A. Y. Katunin, I. I. Lukashevich, V. V. Sklyarevskii, V. V. Suraev, V. V. Filippov, N. I. Filippov, and V. A. Shevtsov, *ZhETF* **89**, 2197 (1985) [*JETP* **62**, 1268 (1985)].
- [19] E. B. Gordon, A. A. Pel'menev, O. F. Pugachev, and V. V. Khmelenko, *Pis'ma Zh. Eksp. Teor. Fiz.* **37**, 235 (1983) [*JETP Lett.* **37**, 282 (1983)].
- [20] S. I. Kiselev, V. V. Khmelenko, and D. M. Lee, *Phys. Rev. Lett.* **89**, 175301 (2002).
- [21] J. H. Constable, J. R. Gaines, P. E. Sokol, and P. C. Souers, *J. Low Temp. Phys.* **58**, 467 (1985).
- [22] G. C. Hancock, C. A. Mead, D. G. Truhlar, and A. J. C. Varandas, *J. Chem. Phys.* **91**, 3492 (1989).
- [23] T. Takayanagi and S. Sato, *J. Chem. Phys.* **92**, 2862 (1990).
- [24] T. Kumada, S. Mori, T. Nagasaka, J. Kumagai, and T. Miyazaki, *J. Low Temp. Phys.* **122**, 265 (2001).
- [25] T. Kumada, M. Sakakibara, T. Nagasaka, H. Fukuta, J. Kumagai, and T. Miyazaki, *J. Chem. Phys.* **116**, 1109 (2002).
- [26] J. Ahokas, J. Järvinen, V. V. Khmelenko, D. M. Lee, and S. Vasiliev, *Phys. Rev. Lett.* **97**, 095301 (2006).
- [27] J. Ahokas, O. Vainio, S. Novotny, J. Järvinen, V. V. Khmelenko, D. M. Lee, and S. Vasiliev, *Phys. Rev. B* **81**, 104516 (2010).
- [28] V. Shevtsov, A. Frolov, I. Lukashevich, E. Ylinen, P. Malmi, and M. Punkkinen, *J. Low Temp. Phys.* **95**, 815 (1994).
- [29] A. I. Strom, K. L. Fillmore, and D. T. Anderson, *Low Temp. Phys.* **45**, 676 (2019).
- [30] L. O. Paulson, F. M. Mutunga, S. E. Follett, and D. T. Anderson, *J. Phys. Chem. A* **118**, 7640 (2014).
- [31] M. E. Balabanoff, M. Ruzi, and D. T. Anderson, *Phys. Chem. Chem. Phys.* **20**, 422 (2018).
- [32] F. M. Mutunga, K. M. Olenyik, A. I. Strom, and D. T. Anderson, *J. Chem. Phys.* **154**, 014302 (2021).

- [33] S. Sheludiakov, D. M. Lee, V. V. Khmelenko, J. Järvinen, J. Ahokas, and S. Vasiliev, *Rev. Sci. Instrum.* **91**, 063901 (2020).
- [34] S. Vasilyev, J. Järvinen, E. Tjukanoff, A. Kharitonov, and S. Jaakkola, *Rev. Sci. Instrum.* **75**, 94 (2004).
- [35] S. Sheludiakov, J. Ahokas, O. Vainio, J. Järvinen, D. Zvezdov, S. Vasiliev, V. V. Khmelenko, S. Mao, and D. M. Lee, *Rev. Sci. Instrum.* **85**, 053902 (2014).
- [36] J. Ahokas, O. Vainio, J. Järvinen, V. V. Khmelenko, D. M. Lee, and S. Vasiliev, *Phys. Rev. B* **79**, 220505(R) (2009).
- [37] I. F. Silvera, *Rev. Mod. Phys.* **52**, 393 (1980).
- [38] L. Andrews and X. Wang, *Rev. Sci. Instrum.* **75**, 3039 (2004).
- [39] I. F. Silvera and J. T. M. Walraven, *Phys. Rev. Lett.* **44**, 164 (1980).
- [40] F. Schmidt, *Phys. Rev. B* **10**, 4480 (1974).
- [41] J. Järvinen, V. V. Khmelenko, D. M. Lee, J. Ahokas, and S. Vasiliev, *J. Low Temp. Phys.* **162**, 96 (2011).
- [42] S. Sheludiakov, D. M. Lee, V. V. Khmelenko, J. Ahokas, J. Järvinen, and S. Vasiliev, *J. Low Temp. Phys.* (2021).
- [43] G. W. Collins, P. C. Souers, J. L. Maienschein, E. R. Mapoles, and J. R. Gaines, *Phys. Rev. B* **45**, 549 (1992).
- [44] S. Sheludiakov, J. Ahokas, J. Järvinen, L. Lehtonen, O. Vainio, S. Vasiliev, D. M. Lee, and V. V. Khmelenko, *Phys. Chem. Chem. Phys.* **19**, 2834 (2017).
- [45] J. Van Kranendonk and G. Karl, *Rev. Mod. Phys.* **40**, 531 (1968).
- [46] C.-Y. Kuo, R. J. Kerl, N. D. Patel, and C. K. N. Patel, *Phys. Rev. Lett.* **53**, 2575 (1984).
- [47] H. Meyer, *Low. Temp. Phys.* **24**, 381 (1998).
- [48] Washburn *et al.*, *J. Low. Temp. Phys.* **40**, 187 (1980).
- [49] V. Shevtsov, E. Ylinen, P. Malmi, and M. Punkkinen, *Phys. Rev. B* **62**, 12386 (2000).
- [50] R. W. Hill and B. W. Ricketson, *Philos. Mag.* **45**, 277 (1954).